THE JOURNAL OF BIOLOGICAL CHEMISTRY VOL. 286, NO. 13, pp. 11659–11671, April 1, 2011

Inactivation of the Mitochondrial Carrier SLC25A25 (ATP-Mg^{2+}/P_i Transporter) Reduces Physical Endurance and Metabolic Efficiency in Mice*

Received for publication, November 15, 2010, and in revised form, January 31, 2011 Published, JBC Papers in Press, February 4, 2011, DOI 10.1074/jbc.M110.203000

Rea P. Anunciado-Koza[1], Jingying Zhang, Jozef Ukropec[2], Sudip Bajpeyi, Robert A. Koza, Richard C. Rogers, William T. Cefalu, Randall L. Mynatt, and Leslie P. Kozak[3]

From the Pennington Biomedical Research Center, Baton Rouge, Louisiana 70808

An ATP-Mg^{2+}/P_i inner mitochondrial membrane solute transporter (SLC25A25), which is induced during adaptation to cold stress in the skeletal muscle of mice with defective UCP1/brown adipose tissue thermogenesis, has been evaluated for its role in metabolic efficiency. SLC25A25 is thought to control ATP homeostasis by functioning as a Ca^{2+}-regulated shuttle of ATP-Mg^{2+} and P_i across the inner mitochondrial membrane. Mice with an inactivated *Slc25a25* gene have reduced metabolic efficiency as evidenced by enhanced resistance to diet-induced obesity and impaired exercise performance on a treadmill. Mouse embryo fibroblasts from *Slc25a25*$^{-/-}$ mice have reduced Ca^{2+} flux across the endoplasmic reticulum, basal mitochondrial respiration, and ATP content. Although *Slc25a25*$^{-/-}$ mice are metabolically inefficient, the source of the inefficiency is not from a primary function in thermogenesis, because *Slc25a25*$^{-/-}$ mice maintain body temperature upon acute exposure to the cold (4 °C). Rather, the role of SLC25A25 in metabolic efficiency is most likely linked to muscle function as evidenced from the physical endurance test of mutant mice on a treadmill. Consequently, in the absence of SLC25A25 the efficiency of ATP production required for skeletal muscle function is diminished with secondary effects on adiposity. However, in the absence of UCP1-based thermogenesis, induction of *Slc25a25* in mice with an intact gene may contribute to an alternative thermogenic pathway for the maintenance of body temperature during cold stress.

Obesity and its associated co-morbidities develop from a prolonged energy imbalance that occurs when food intake exceeds energy expenditure. Although considerable progress has been made in our understanding of the food intake side of the energy balance equation (1), much less is known of mechanisms of energy expenditure that can be utilized to reduce a positive energy balance. Two major thermogenic systems are known that can be activated voluntarily to increase energy expenditure. One is brown adipose tissue that functions to regulate body temperature and will be activated or not depending in part on whether a person chooses to become exposed to and to tolerate a reduced ambient temperature. The other is skeletal muscle, which functions primarily for motility, but is a major site for caloric expenditure and can be recruited to reduce excessive caloric stores. Although either exposure to reduced ambient temperature or physical activity can increase energy expenditure to maintain energy balance (2, 3), the modern lifestyle of many individuals does not support these natural anti-obesity solutions.

Given that skeletal muscle comprises up to 40% of total body weight and is able to consume 90% of the whole body oxygen uptake during maximal physical activity (4), the positive energy balance of obese individuals could be determined by variations in the efficiency of muscle energy metabolism (5). Mutations to several genes encoding and/or regulating the sarcoendoplasmic reticulum Ca^{2+}-ATPases (SERCAs)[4] show deleterious phenotypes caused by defective Ca^{2+} cycling, energy metabolism, and muscle function (6–8); however, very few of these mutations have been analyzed for their impact on susceptibility to obesity and type 2 diabetes. Although the suppression of oxidative phosphorylation by reducing the number of mitochondria has been proposed to provide the conditions for the development of obesity and type 2 diabetes (5), in fact such suppression, as occurs with a skeletal muscle-specific inactivation of PGC-1α, leads to mice with a lean body composition and resistance to diet-induced obesity (9). Therefore PGC-1α-deficient mice are similar to UCP1-deficient mice in that a reduction in the capacity for energy expenditure and reduced mitochondrial function paradoxically reduces susceptibility to environmental obesity (10).

It is generally observed that the inactivation of genes of energy metabolism causes reduced metabolic efficiency, that is, the mutant mouse is more resistant to the effects of an obesogenic environment (3). The survival of a mouse in the wild depends on maximal metabolic efficiency. A mouse can adapt to the loss of a gene by utilizing alternative pathways; however, it is highly probable that the pathway now functions with reduced efficiency. For example, the targeted inactivation of mitochondrial uncoupling protein (UCP1) illustrates how loss

* This work was supported, in whole or in part, by National Institutes of Health Grants R01-HD008431 (to L. P. K.) and 1P30 DK07246.

[1] Present address: Taconic Farms, One Hudson City Center, Hudson, NY 12534.

[2] Present address: Institute of Experimental Endocrinology, Slovak Academy of Sciences, Bratislava, Slovak Republic.

[3] Present address: Polish Academy of Sciences in Olsztyn, ul. Tuwima 10, 10-747 Olsztyn, Poland. To whom correspondence should be addressed. Tel.: 48-89-523-46-86; Fax: 48-524-01-24; E-mail: l.kozak@pan.olsztyn.pl.

[4] The abbreviations used are: SERCA, sarcoendoplasmic reticulum Ca^{2+}-ATPase; UCP, uncoupling protein; MEF, mouse embryonic fibroblast; MC, mitochondrial carrier; ScaMC, short calcium-binding MC; FCCP, carbonyl cyanide 4-(trifluoromethoxy)phenylhydrazone; KO, knock-out; ER, endoplasmic reticulum; RER, rough endoplasmic reticulum; Gdm, mitochondrial glycerol-3-phosphate dehydrogenase.

of this function for maintaining body temperature is not lethal in the laboratory environment and mice can be adapted to a severely reduced ambient temperature (4 °C). However, the alternative mechanism, which compensates for the lack of UCP1, produces heat at an increased caloric cost that is observed by a reduction in adipose stores during diet-induced obesity (10).

Using microarray and gene expression analysis of skeletal muscle from mice with mutations in *Ucp1* and *Lep* we now show that *Slc25a25*, which encodes a Ca^{2+}-sensitive ATP-Mg^{2+}/P_i carrier in the inner mitochondria, is consistently up-regulated in the skeletal muscle and inguinal fat in a number of cold-adapted UCP1-deficient mouse models. Therefore, up-regulation of *Slc25a25* in models of UCP1 deficiency is associated with adaptation to protect body temperature, but the caloric cost, evident by a resistance to diet-induced obesity, reflects a reduction in metabolic efficiency. To elucidate the function of SLC25A25 in energy balance, mice with a global deletion of *Slc25a25* were created and shown to be resistant to diet-induced obesity and have reduced physical endurance on a treadmill. Therefore, reduced metabolic efficiency occurs with both over- and underexpression of *Slc25a25*. Because SLC25A25 is thought to maintain ATP homeostasis by functioning as a Ca^{2+}-regulated shuttle of ATP-Mg^{2+} and P_i across the inner mitochondrial membrane (11), SLC25A25 is proposed to play an important function in the regulation of ATP homeostasis necessary to support Ca^{2+} cycling in skeletal muscle. Its absence leads to energy inefficiency in the performance of work, with secondary consequences on overall adiposity.

EXPERIMENTAL PROCEDURES

Gene Targeting—The Cre/loxP system was used to generate mice with a global *Slc25a25* deletion (Fig. 2*A*). A floxed *Slc25a25* allele was created by introducing loxP sites into the introns flanking exons 2 and 3, with the third loxP site flanking a neo cassette (G418 resistance) as a selectable marker. Targeted C57BL/6J embryonic stem cells carrying the conditional floxed allele were introduced into C57BL/6J-Tyr c-2J host blastocyts. Chimeric progeny were crossed with C57BL/6J-Tyrc-2J mice to generate progeny heterozygous for the targeted allele. The presence of the 3 loxP sites was validated by genomic PCR (Fig. 2*B*). Mice with a global deletion of *Slc25a25* were generated by breeding $Slc25a25^{fl/fl}$ to *EIIa-Cre* mice that express *Cre* under the control of the *EIIa* promoter leading to expression of *Cre* recombinase in preimplantation embryos. The expression of genes under control of the adenoviral *EIIa* promoter is known to be restricted to the oocytes and preimplantation stages of the embryo (12), thereby leading to excision of exons 2 and 3 in the germline and all subsequent tissues and progeny. Progeny carrying the complete deletion were backcrossed to wild type C57BL/6J (WT) mice to ensure germline transmission of the mutation and removal of the *EIIa-Cre* transgene.

Microarray Analysis—Total RNA isolated from gastrocnemius red muscle of leptin-treated and untreated (PBS) $Ucp1^{-/-}$·$Lep^{-/-}$ mice were used. RNA isolation was performed as previously described (13). Mice were kept at 28 °C for 1 week, and then ambient temperature was reduced 2 °C daily. Mice received leptin (1 μg/g/day in divided doses at 8:30 a.m. and 4:30 p.m.) from 20 °C until 16 °C. Animals were sacrificed 24 h after ambient temperature reached 16 °C. Quality of RNA was determined using the Agilent 2100 Bioanalyzer. RNA integrity number of samples ranged from 8.1 to 8.8. Each RNA sample was labeled and hybridized to the Applied Biosystems Mouse Genome Survey Microarray platform. Each microarray contained ~34,000 features that include a set of about 1,000 controls. Each microarray used 32,096 probes to interrogate 32,281 curated genes representing 44,996 transcripts. Labeling and hybridization were performed as described previously (14). Signal intensities across microarrays were normalized by trimmed means. Features with signal/noise values >3 and quality FLAG values <5000 were considered "detected" and subjected to analysis of variance with p value of 0.01 using Spotfire Decision Site software (Spotfire, Somerville, MA). The complete list of genes with statistically significant ($p < 0.05$) levels of induction by leptin is shown in Table 1.

Molecular Cloning and DNA Sequence of Mouse Skeletal Muscle Slc25a25—cDNA was prepared from leptin-treated $Ucp1^{-/-}$·$Lep^{-/-}$ quadriceps muscle. *Slc25a25* NCBI reference sequence NM146118 was used to design primers for PCR using cDNA prepared from $Ucp1^{-/-}$·$Lep^{-/-}$ quadriceps muscle. Final reaction products were phenol-chloroform extracted and ethanol-precipitated. DNA was cut with appropriate restriction enzymes, gel-purified, and subcloned to the pCI-neo mammalian expression vector (Promega, Madison, WI). Nucleotide sequence was verified and aligned with mouse major isoform (NM146118). *Slc25a25* sequence from $Ucp1^{-/-}$·$Lep^{-/-}$ quadriceps muscle corresponded to NCBI reference sequence AK132201, which lacks exon 6 and corresponds to the human SCaMC-2b spliced variant.

Animals and Study Design—Experiments were carried out on C57BL/6J (WT) and $Slc25a25^{-/-}$ male mice maintained in a temperature-controlled room (28 °C) with a 12-h light/12-h dark cycle and fed rodent chow (PicoLab Rodent Diet 20 with 12 kcal % fat, LabDiet, Richmond, IN). Mice carrying a conditional floxed *Slc25a25* allele were generated by the Pennington Transgenic Core. All animal experiments were approved by the Pennington Biomedical Research Center Institutional Animal Care and Use Committee in accordance with National Institutes of Health guidelines for care and use of laboratory animals.

Dietary Studies—Eight-week-old *Slc25a25* WT and knockout male mice previously maintained at 28 °C and fed chow diet (PicoLab Rodent Diet 20 with 12 kcal % fat) were single-housed, fed a high fat diet (D12331 with 58 kcal % fat, Research Diets Inc., New Brunswick, NJ), and kept at 20 °C for 10 weeks. Mice were subsequently maintained at 28 °C for another 10 weeks. In another study, two groups of 8-week-old WT mice were fed chow and a high fat diet at 23 °C for 30 weeks.

Phenotypes of Energy Balance—Body composition was analyzed by NMR (Minispec body composition analyzer, Bruker Optics, Billerica, MA). Oxygen consumption, carbon dioxide production, and physical activity of individual mice were measured in a 16-chamber Oxymax lab animal monitoring system CLAMS (Columbus Instruments, Columbus, OH). Glucose tolerance and insulin tolerance tests were performed after an overnight fast as previously described (13).

Cold Exposure—Slc25a25 WT and knock-out mice maintained at 28 °C were single-housed in cages with corncob bedding and exposed to ambient temperature of 4 °C, and body temperature was measured with a rectal probe (TH-8, Physitemp Instruments Inc., Clifton, NJ).

Assessment of Exercise Endurance—Untrained, age- and body weight-matched male mice were used in forced exercise endurance testing using a six-lane motorized rodent treadmill (Columbus Instruments, Columbus, OH). Mice were acclimatized to the treadmill for 4 days at a velocity of 8 m/min for 15 min. On day 5, exercise endurance was tested at an initial velocity of 8 m/min for 1 min after which velocity was increased at 2-m/min increments every minute until a maximum velocity of 14 m/min. Exhaustion was determined as the point at which the animal would repeatedly fall onto the metal grid despite gentle tapping on the back of the mouse.

Quantitative Reverse Transcription-PCR—Total RNA was prepared from tissues homogenized in TRI reagent (Molecular Research Center Inc., Cincinnati, OH) as described previously (15). The gastrocnemius is divided into 2 parts, the outer gastrocnemius white and the inner gastrocnemius red. The gastrocnemius white is located on the superficial lateral and medial portions, whereas the red part is in the deep medial and lateral portions. Quantitative reverse transcription-PCR was performed using total RNA with specific primers and probes designed using Primer-Express™, version 2.0.0 (Applied Biosystems, Foster City, CA). TaqMan probes were used for quantification of genes using the TaqMan one-step reverse transcriptase PCR master mixture (Applied Biosystems). All of gene expression data were normalized to the level of cyclophilin B for mouse studies, RPLPO for human studies, or total nanograms of input RNA/reaction. Primer and probe sequences are available upon request. Probes were designed from sequences in the C-terminal region to detect all 4 isoforms of human SLC25A25 (hSCaMC-2a to 2d).

Mouse Embryonic Fibroblasts—Mouse embryonic fibroblasts (MEF) were generated from *Slc25a25* WT and knock-out E13.5 embryos. Carcasses were eviscerated, decapitated, and finely minced. Tissue from each embryo was digested with 0.05% trypsin for 15 min at 37 °C, washed with 10% FBS/DMEM, centrifuged at 1,000 × *g* for 5 min, and the supernatant discarded. Cell pellet was re-suspended and cultured in DMEM plus 10% FBS and penicillin-streptomycin. Genotype of each embryo was validated by genomic PCR. Primary MEF up to passage 7 were used for experiments.

Calcium Mobilization Assay—MEF were seeded at a density of 30,000 cells/well and incubated overnight at 37 °C. Medium was replaced with Hanks' balanced salt solution buffer and an equal volume of loading buffer with fluorescent dye (FLIPR Calcium Assay Kit, Molecular Devices, Sunnyvale, CA) and 25 mM probenecid was added. Cell plates were then incubated for 1 h at 37 °C and then for 45 min at RT protected from light. Changes in cytoplasmic calcium concentration in response to 300 nM bradykinin, 1 μM thapsigargin, and 5 μM ionomycin were recorded as relative fluorescence units using the FlexStation fluorescence plate reader (Molecular Devices). Probenecid, bradykinin, thapsigargin, and ionomycin were from Sigma.

Cellular Metabolism—The XF24 Analyzer (Seahorse Bioscience, Billerica, MA) was used to measure the oxygen consumption rate in a 24-well format (16). Culture medium was replaced with unbuffered DMEM supplemented with 25 mM glucose, 0.5 mM glutamine, and 1 mM pyruvate 1 h prior to assay. Optimum number of cells for bioenergetic experiments was initially determined with MEF seeded at different densities (25,000, 30,000, 35,000, and 40,000 cells/well). We used 30,000 cells/well for subsequent experiments. Mitochondrial function in MEF was determined through sequential addition of 5 μM oligomycin, 1 μM carbonyl cyanide 4-(trifluoromethoxy)phenylhydrazone (FCCP), and 1.5 μM antimycin A, 1 μM rotenone. This allowed determination of basal oxygen consumption, oxygen consumption linked to ATP synthesis, non-ATP linked oxygen consumption (proton leak), uncoupled respiration, and non-mitochondrial oxygen consumption (17, 18). Oligomycin-sensitive respiration is calculated from the mean of the four measurements after addition of oligomycin. ATP synthesis-linked oxygen consumption is the difference between basal respiration and oligomycin-sensitive respiration. Proton leak is the difference between oligomycin-sensitive respiration and respiration after injection of antimycin A and rotenone. Non-mitochondrial respiration is residual respiration obtained from the mean of least three points after addition of antimycin A and rotenone. Uncoupled respiration was calculated as the mean of the first three points after FCCP addition. Protein content in each well was measured to confirm an equal number of cells per well. Protein concentrations were determined by bicinchoninic acid assay (Sigma). Oligomycin, FCCP, antimycin A, and rotenone were from Sigma.

ATP Measurements—ATP levels in wild type and SLC25A25-deficient MEF were determined using an ATPlite Luminescence Assay System (PerkinElmer Life Sciences). Cells were seeded at a density of 30,000 cells per well in unbuffered DMEM supplemented with 25 mM glucose, 0.5 mM glutamine, and 1 mM pyruvate, and incubated in a non-CO_2 incubator at 37 °C for 1 h. Cells were then exposed to the following compounds for 1 min: 5 μM oligomycin, 1 μM FCCP, 100 mM 2-deoxy-D-glucose, 2 μM rotenone, and 25 μM carboxyatractyloside. Cells were lysed and cellular ATP content was measured. Luminescence intensity of each well was measured using a Berthold EG&G MicroLumat Plus DL Ready plate-reading luminometer.

Cell Viability—The viability of the MEF following a 1-min exposure to test compounds was assessed using the CellTiter-Blue Cell Viability Assay (Promega, Madison, WI). The fluorescence intensity of each well was measured using a FlexStation fluorescence plate reader (Molecular Devices).

Muscle Fiber-type Analysis—Skeletal muscle fiber-type was analyzed using a immunohistochemistry technique modified from Bajpeyi *et al.* (19). In brief, soleus muscle were collected, cleaned, and blotted dry prior to mounting in a mixture of optimal cutting temperature compound and tragacanth powder and then frozen in isopentane cooled over liquid nitrogen. Twelve-μm sections were processed for immunohistochemical staining. Muscle sections were incubated in blocking buffer (donkey serum) for 2 h followed by overnight incubation at 4 °C in primary antibodies (1:200, v/v) specific for myosin slow muscle (MAB1628, Chemicon) and laminin (AB2500, Abcam Inc.,

TABLE 1
Microarray gene expression data in gastrocnemius red muscle of Ucp1$^{-/-}$·Lep$^{-/-}$ mice treated with leptin

Gene	*p* value	Lep(+)/Lep(−)
		Fold-change
Ion transport		
Slc25a25, ATP-Mg^{2+} mitochondrial carrier	0.001	3.3
Solute carrier family 20, member 2	0.047	2.4
Calcium channel, voltage-dependent γ subunit 6	0.039	2.1
ATPase, H^+ transporting, lysosomal accessory protein 2	0.032	1.5
Protein translocation		
Exportin	0.031	2.4
Mitochondrial enzyme		
Aldehyde dehydrogenase family 7, member A1	0.009	3.3
Thioredoxin reductase 2	0.014	2.0
Phosphate metabolism		
Paraoxonase 20.012	2.6	
Peroxisomal/mitochondrial enzyme		
Catalase	0.006	1.5
Serine hydrolase-like	0.046	1.8
Transcription factors		
GCN5 general control of amino acid synthesis-like 2 (yeast)	0.030	4.1
Zinc finger protein 295	0.030	3.8
Homeo box A5	0.012	2.4
cAMP responsive element binding protein 1: RIKEN cDNA 3526402H1 gene	0.027	2.2
Metal response element-binding protein transcription factor 2	0.006	1.8
TGFβ inducible early growth response 3	0.042	2.0
Core promoter element-binding protein	0.020	1.8
Stress and muscle fiber type		
Heat shock protein 1 (chaperonin)	0.038	1.7
Wnt signaling related proteins		
Dishevelled, dsh homolog 1 (Drosophila)	0.035	2.1
Transducin-like enhancer of split 4, homolog of *Drosophila* E (spl)	0.006	1.9
PAI regulation		
Vitronection	0.005	2.0
Angiogenesis and obesity		
Vascular endothelial growth factor A	0.012	1.7
Lipid mediator, inflammation		
Leukotriene A4 hydrolase	0.018	2.0
Carbohydrate metabolism		
Phosphofructokinase, muscle	0.033	1.7
Sorbitol dehydrogenase 1	0.010	1.6
Intracellular lipid storage		
Adipose differentiation related protein	0.016	2.0
Adipocyte differentiation		
Cyclin D1	0.004	2.0
Fatty acid oxidation		
Hydroxyacyl-coenzyme A dehydrogenase/3-ketoacyl-coenzyme A thiolase/ enoyl-coenzyme A hydratase (trifunctional protein), α subunit	0.046	1.9
Endoplasmic reticulum calcium-binding protein		
Reticulocalbin	0.026	1.5

Cambridge, MA). After washing with phosphate-buffered saline, sections were incubated in the secondary antibodies (Alexa Fluor 680 donkey anti-mouse and Alexa Fluor 350 donkey anti-rat at 1:200 and 1:500 (v/v) dilution, respectively, from Invitrogen) for 2 h. After further washing, the sections were mounted in permount and coverglass was applied. Images were taken using confocal microscope (Zeiss 510 META, Carl Zeiss, Thornwood, NY) and type I fibers were counted. The relative numbers of the different fiber types were quantified by counting 2–3 sections from each sample containing a minimum of 50 muscle fibers.

Statistical Analysis—The data are expressed as the mean ± S.E. Unpaired *t* test was used to compare differences between groups. Analysis of variance with the Bonferroni post hoc test was used when more than two groups were compared (Statview, version 5.0.1; SAS Institute Inc., Cary, NC).

RESULTS

Microarray and Gene Expression Analysis of Skeletal Muscle for Genes Associated with Induction of Thermogenesis—The body temperature of *Ucp1*$^{-/-}$ or *Lep*$^{-/-}$ mice drops 10 °C within 3 h when they are acutely exposed to an ambient temperature of 5 °C. If the ambient temperature is gradually reduced about 2 degrees/day both mutant mice can tolerate the cold at 5 °C for weeks (20, 21). Double mutant *Ucp1*$^{-/-}$·*Lep*$^{-/-}$ mice are not able to tolerate the cold under this protocol of gradually reducing the ambient temperature; however, they can be rescued, if they are administered leptin as the ambient temperature is gradually reduced (22). A microarray analysis was performed on skeletal muscle RNA from *Ucp1*$^{-/-}$·*Lep*$^{-/-}$ mice with and without treatment with leptin to identify inducible thermogenic pathways. Table 1 provides a

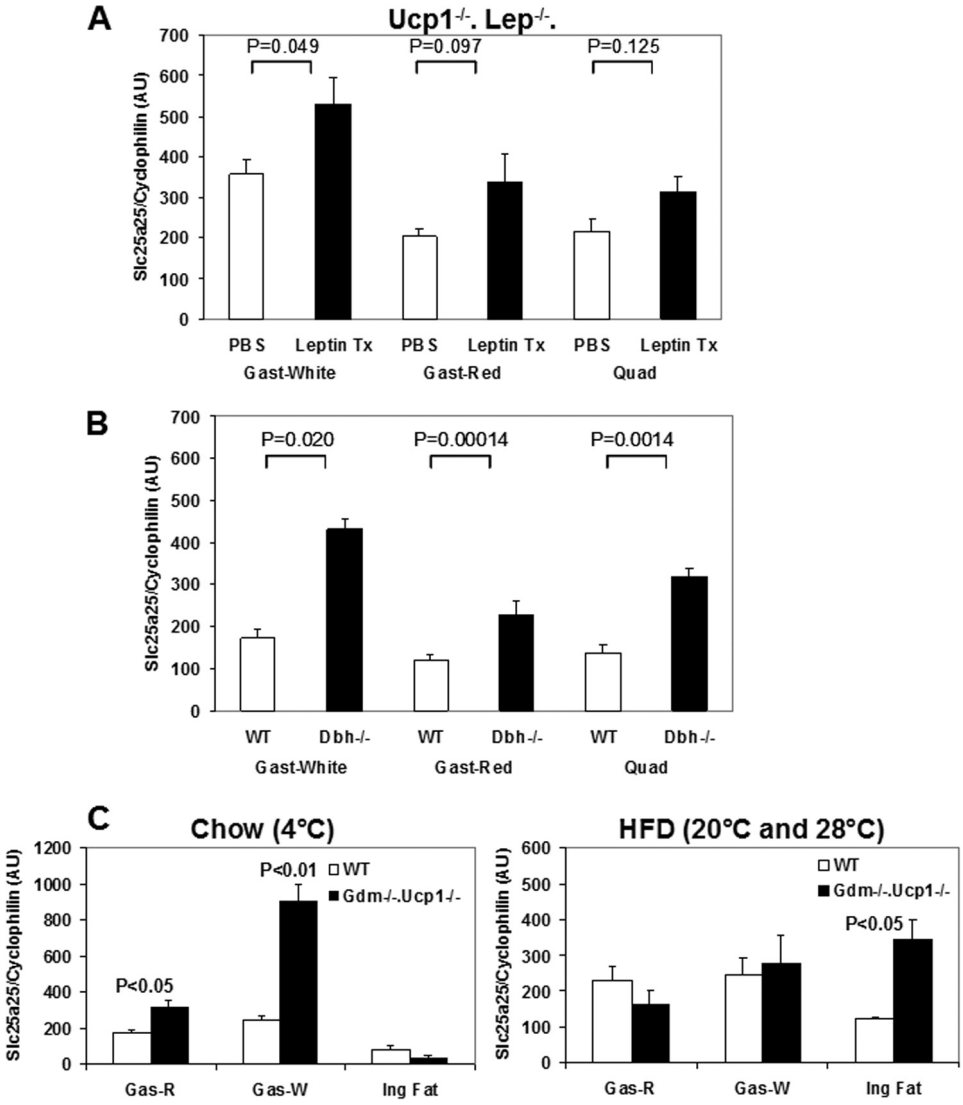

FIGURE 1. **Gene expression of *Slc25a25* in UCP1-deficient mouse models.** *A*, gene expression in skeletal muscle of PBS and leptin-treated $Ucp1^{-/-}$·$Lep^{-/-}$ mice adapted to 20 °C. *Gast* is gastronemius muscle. Muscle dissection is described under "Experimental Procedures." *B*, gene expression in skeletal muscle of $Dbh^{-/-}$ (dopamine β-hydroxylase) mice adapted to 16 °C. *C*, gene expression in skeletal muscle and inguinal fat in $Gdm^{-/-}$ (mitochondrial glycerol-3-phosphate dehydrogenase) mice fed chow diet adapted to 4 °C and in high fat diet fed (*HFD*) mice were housed at 20 °C for 10 weeks and then at 28 °C for 10 weeks.

list of 29 genes with significant levels of induction. That 5 of these genes are associated with Ca^{2+} metabolism in skeletal muscle underscores the pivotal role for this metabolism in the induction of thermogenesis by leptin. We selected Slc25a25, which encodes a ATP-Mg^{2+}/inorganic phosphate carrier located in the inner mitochondrial membrane, for further analysis, because it is structurally analogous to UCP1 and may have a related transport function. Up-regulation of *Slc25a25* (ATP-Mg^{2+}/P_i carrier) consistently occurs in skeletal muscle of other cold-adapted UCP1-deficient mouse models, including, induction in $Ucp1^{-/-}$·$Lep^{-/-}$ (Fig. 1*A*), $Dbh^{-/-}$ (dopamine β-hydroxylase) (Fig. 1*B*), and $Gdm^{-/-}$·$Ucp1^{-/-}$ (Gdm; mitochondrial glycerol-3-phosphate dehydrogenase) mice (Fig. 1*C*). SLC25A25 is thought to maintain ATP homeostasis by functioning as a Ca^{2+}-regulated shuttle of ATP-Mg^{2+} and P_i across the inner mitochondrial membrane (11), however, the induction of *Slc25a25* expression under severe cold stress suggests that SLC25A25 is able to contribute to thermogenesis in skeletal muscle and inguinal fat. How this thermogenic activity is achieved by the putative function of SLC25A25 as an inner mitochondrial solute transporter is not understood.

The DNA sequence analysis of the *Slc25a25* isoform induced in muscle was performed on a cDNA cloned from leptin-treated $Ucp1^{-/-}$·$Lep^{-/-}$ quadriceps muscle. The *Slc25a25* isoform overexpressed in skeletal muscle of UCP1-deficient mouse models corresponded to the human SCaMC-2b spliced variant lacking exon 6.

Generation and Validation of Global Slc25a25 Knock-out Mice—To determine the role of *Slc25a25* in overall energy homeostasis, we used the Cre/loxP system to generate mice with a global *Slc25a25* deletion as described under "Experimental Procedures" (Fig. 2*A*). Mice with a global deletion of *Slc25a25* were generated by breeding $Slc25a25^{fl/fl}$ to *EIIa-Cre* mice leading to *Slc25a25* excision in the germline and all subsequent tissues and progeny (Fig. 2*B*). At 28 °C ambient temperature, newborn

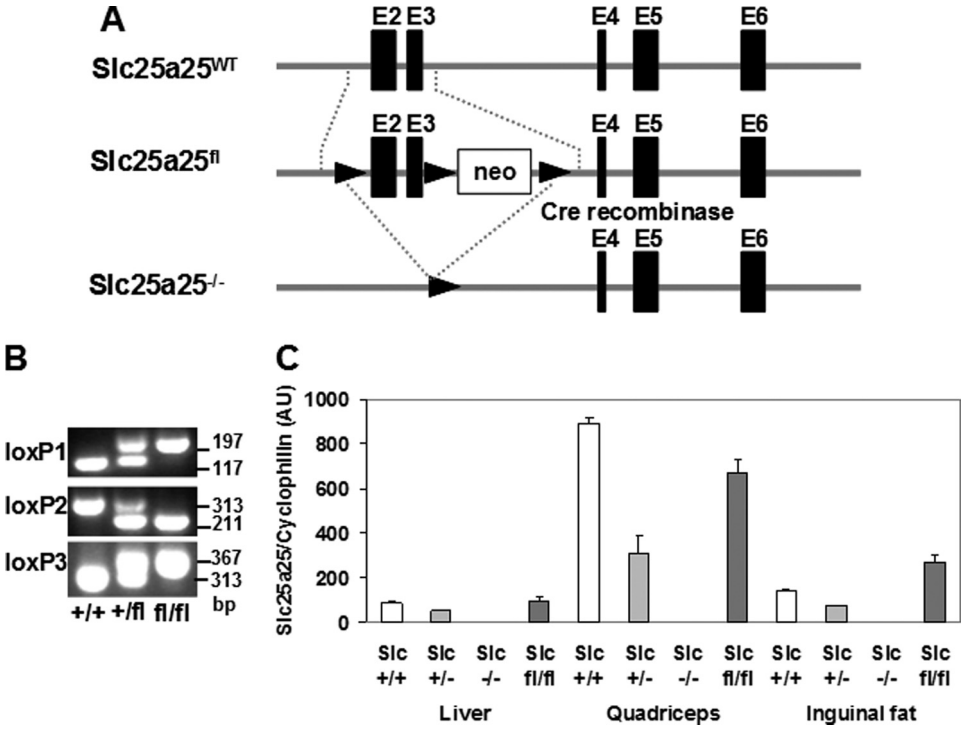

FIGURE 2. **Generation and validation of *Slc25a25* knock-out mice.** *A*, scheme describing generation of *Slc25a25* knock-out. *Rectangles* and *triangles* correspond to exons and loxP sites, respectively. *B*, genomic PCR to demonstrate the presence of 3 loxP sites in *Slc25a25* wild-type, heterozygous floxed, and homozygous floxed mice. *C*, gene expression profile in liver, quadriceps, and inguinal fat showing *Slc25a25* gene expression in wild-type ($n = 3$) and floxed mice ($n = 3$); and a reduction and absence of expression in heterozygotes ($n = 3$) and knock-out ($n = 3$) mice, respectively. Data are mean ± S.E.

Slc25a25$^{-/-}$ progeny are viable, born at the expected Mendelian ratio and fertile. Gene expression for *Slc25a25* in liver, quadriceps, and inguinal fat measured by qRT-PCR showed similar levels in expression in WT and *Slc25a25*$^{fl/fl}$ mice, intermediate expression in *Slc25a25*$^{+/-}$ mice, and absence of expression in *Slc25a25*$^{-/-}$ mice (Fig. 2*C*). Importantly, expression in each tissue was proportional to the number of intact alleles.

Body Weight Regulation and Metabolic Efficiency in Slc25a25$^{-/-}$ *Mice*—At weaning (24 days of age) there was no difference in body weight or composition in *Slc25a25*$^{+/-}$ or *Slc25a25*$^{-/-}$ mice raised by mothers fed a chow diet (~12 Kcal % fat) at 28 °C ambient temperature. During the subsequent 5 weeks of development, mutant mice began to show slight, but significant, reductions in both fat and fat-free (lean) mass (Fig. 3*A*). Mice at 8 weeks of age were then fed a high fat diet and maintained first at 20 °C and then at 28 °C (Fig. 3*B*). We predicted that if SLC25A25 is a part of a thermogenic mechanism that is involved in the regulation of body temperature, reductions in adiposity in the KO mice will be robust at 20 °C and then disappear when the ambient temperature is increased to 28 °C, as we previously observed for *Ucp1*$^{-/-}$ mice (10, 13). Similar to the *Ucp1*$^{-/-}$ mice, at 20 °C fat mass gain was much lower in *Slc25a25*$^{-/-}$ than WT mice; however, the phenotype of *Slc25a25*$^{-/-}$ mice deviated from *Ucp1*$^{-/-}$ mice in 2 ways (Fig. 3*B*). First, fat mass remained much lower in *Slc25a25*$^{-/-}$ mice when the ambient temperature was increased to 28 °C and second, lean mass was lower in the *Slc25a25*$^{-/-}$ mice at both 20 and 28 °C. *Ucp1*$^{-/-}$ mice did not have reduced lean mass (13).

Comparisons of body weight and composition of wild type and *Slc25a25*$^{-/-}$ mice suggested that the capacity for growth and maintenance of both fat and fat-free mass is attenuated when the mice are placed on a high fat diet. To assess this phenotype further we calculated metabolic efficiency from body weight and food intake data (Table 2). Food intake was about 10% higher in WT than KO mice at 28 °C but not different at 20 °C. Metabolic efficiency increased 2.1- and 2.2-fold for WT and KO, respectively, in the transition from 20 to 28 °C, indicating that the effects of ambient temperature were similar for WT and KO mice; however, at 20 °C metabolic efficiency was 1.45-fold greater in WT than in KO mice and at 28 °C it was 1.35-fold higher in Wt than KO mice. This suggests that inactivation of *Slc25a25* reduces metabolic efficiency and leads to a reduction in both fat and fat-free mass. Whether metabolic efficiency is reduced in aging mice on a low fat diet is not known, but should be investigated. Young adult *Slc25a25*$^{-/-}$ mice maintained a normal body temperature when acutely exposed to the cold at 4 °C (data not shown), indicating that SLC25A25 is not required for the normal regulation of body temperature. At 18 weeks, described in Fig. 3*B*, glucose tolerance and insulin tolerance tests showed no difference in insulin resistance between wild type and *Slc25a25*$^{-/-}$ mice (data not shown).

Indirect Calorimetry in Slc25a25 Knock-out Mice Indicates Reduced Metabolic Efficiency in the Context of Diet-induced Obesity—As shown in Fig. 3*A*, slight, but significant reductions, in fat mass can be detected in *Slc25a25*$^{-/-}$ mice fed a low-fat chow diet. Energy expenditure in high fat fed mice was not different in KO and wild type mice maintained at 28 °C, but upon the shift to 4 °C oxygen consumption increased about 300% in both genotypes (Fig. 4*A*), consistent with indistinguishable cold-sensitive phenotypes in wild type and KO mice, that

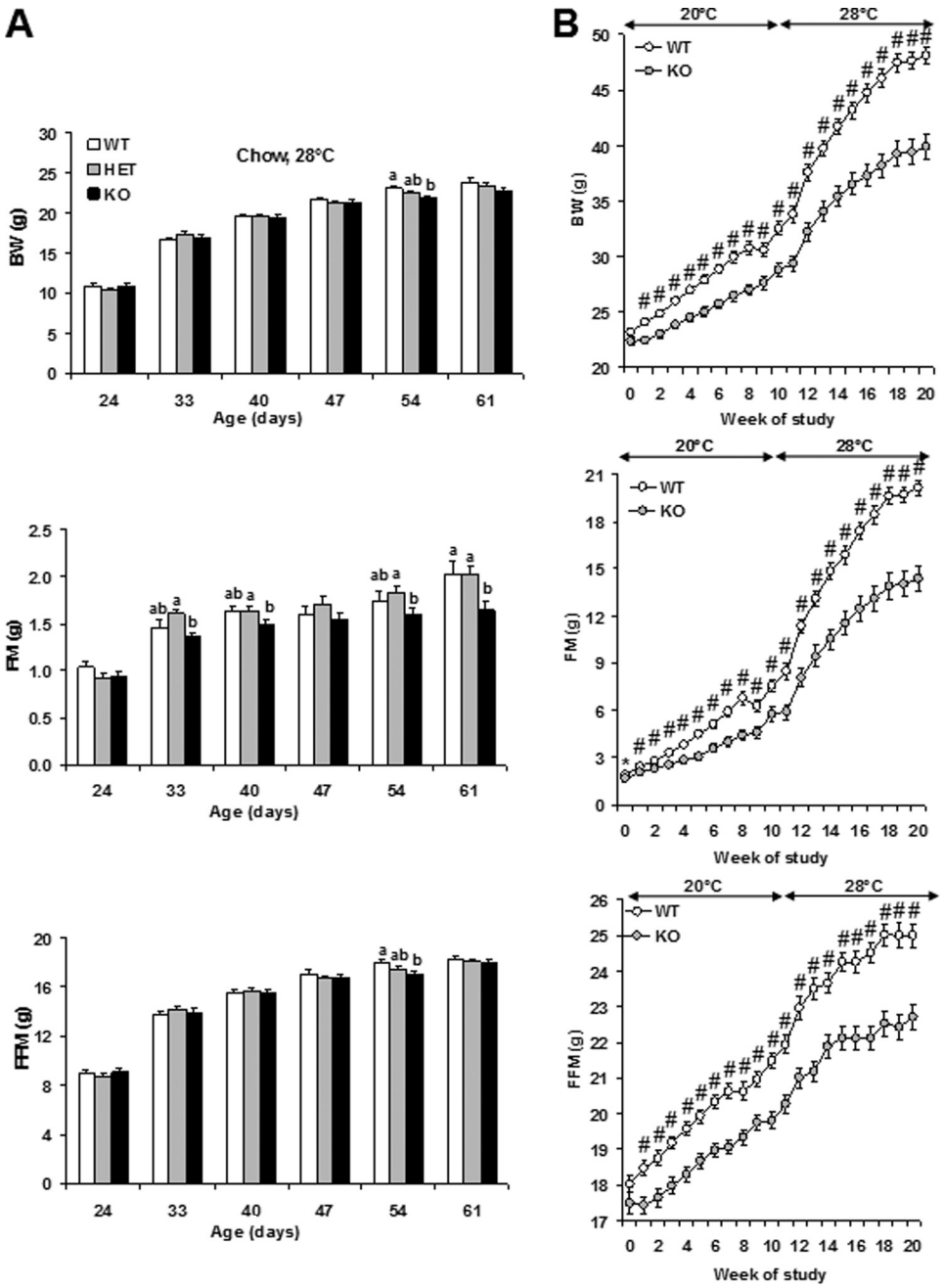

FIGURE 3. **Body weight and body composition in *Slc25a25* wild-type (*WT*), heterozygous (*HET*), and KO mice.** *A*, body weight, fat mass, and fat-free mass in *Slc25a25* WT ($n = 9–13$), heterozygotes ($n = 14–22$), and KO ($n = 9–22$) mice fed chow diet and kept at 28 °C ambient temperature. Data are mean ± S.E. *a* and *b*, with different superscripts are significantly different at $p < 0.05$. *B*, body weight, fat mass and fat-free mass in *Slc25a25* WT ($n = 18$) and KO ($n = 11$) mice a fed high fat diet, and kept at 20 and 28 °C ambient temperature for 20 weeks. Data are mean ± S.E. $p < 0.01$; #, WT *versus* KO.

TABLE 2
Food intake, body weight gain, and metabolic efficiency

	20 °C	28 °C
BW gain (g)	Weeks 2 to 7	Weeks 11 to 20
WT	5.6 ± 0.4[a] (22)	15.2 ± 0.7[a] (14)
KO	3.83 ± 0.4 (20)	11.1 ± 0.5 (11)
Total food intake (g)		
WT	131.5 ± 2.5 (22)	175 ± 4.6[a] (11)
KO	126.6 ± 2.7 (20)	156 ± 3.2 (6)
Metabolic efficiency		
WT	4.2 ± 0.3[a] (22)	8.8 ± 0.2[a] (11)
KO	2.9 ± 0.02 (20)	6.5 ± 0.3 (6)

[a] $p < 0.01$, WT *versus* KO. Metabolic efficiency = body weight gain (g)/ food intake (g) × 100. Data are mean ± S.E.

is, mice of both genotypes housed at 28 °C were able to maintain body temperature when acutely exposed to an ambient temperature of 5 °C for up to 17 h.[5] The data on RER showed the expected reduction (increased fat oxidation) in mice when maintained at 4 °C, but no biologically significant difference in RER between wild type and *Slc25a25*$^{-/-}$ mice. It is unlikely that the slight increase observed in heterozygote mice only has any biological significance (Fig. 4*A*). On the other hand, oxygen consumption was slightly higher in *Slc25a25*$^{-/-}$ mice fed a high fat diet at 4 °C, and at 20 and 28 °C than in wild-type mice

[5] R. P. Anunciado-Koza and L. P. Kozak, unpublished data.

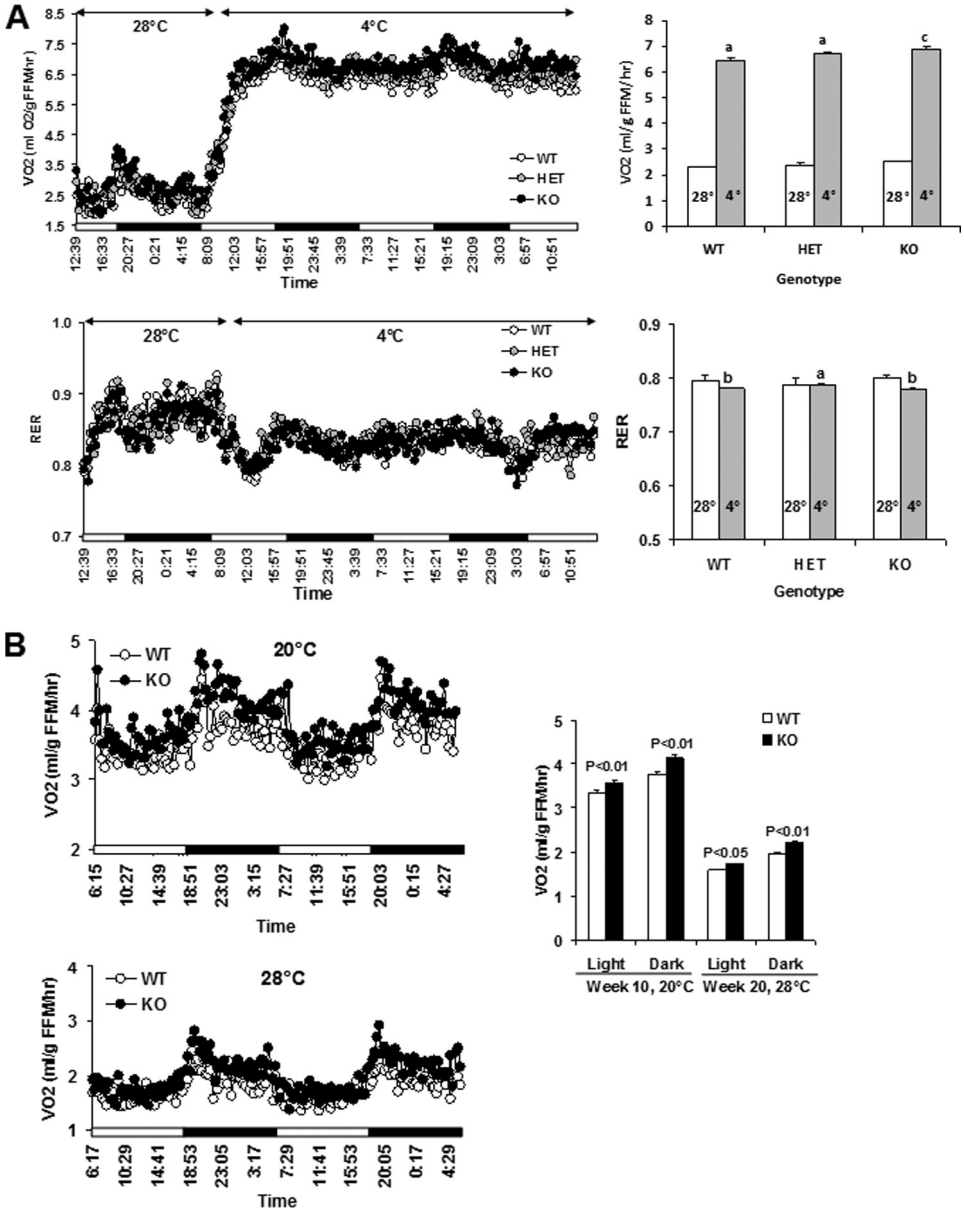

FIGURE 4. **Oxygen consumption and RER in *Slc25a25* wild-type (*WT*) and KO mice.** *A*, VO_2 consumption and RER in 9-week-old WT ($n = 5$), heterozygous ($n = 6$), and KO ($n = 5$) mice fed a high fat diet for 8 days and exposed to 4 °C for 56 h. *Bar graphs* represent VO_2 and RER for 24 h at 28 °C and 48 h at 4 °C. Data are mean ± S.E. *a-c*, means are statistically significant at $p < 0.05$. *B*, VO_2 consumption in WT ($n = 8$) and KO ($n = 8$) mice fed high fat diet at 20 and 28 °C ambient temperature. *Bar graph* represents VO_2 during light and dark hours for 3 days on week 10 at 20 °C and for 3 days on week 20 at 28 °C. Data are mean ± S.E.

during long-term feeding of a high fat diet (Fig. 4*B*). This is different from the response of *Ucp1*$^{-/-}$, which showed differences in diet-induced obesity at 4 and 20 °C, but not at 28 °C, and no genotype-dependent differences in oxygen consumption until the temperature was well below 20 °C (13, 23). Accordingly, between 28 and 20 °C the effects of inactivation of *Slc25a25* on energy expenditure are stronger than those seen in *Ucp1*$^{-/-}$ mice where oxygen consumption does not exceed that of control mice until the ambient temperature is reduced to about 12 °C (23). Whatever physiological pathway SLC25A25 is involved in, it does not seem to be directly associated with thermogenesis regulating body temperature. Furthermore, the levels of *Ucp1* mRNA in interscapular brown adipose tissue from wild type, *Slc25a25*$^{+/-}$, and *Slc25a25*$^{-/-}$ mice expressed as arbitrary units relative to cyclophilin mRNA were 14.1 ± 0.4 ($n = 9$), 13.6 ± 0.9 ($n = 9$), and 12.7 ± 0.9 ($n = 11$), respectively; differences were not statistically significant.

Altered Exercise Endurance in Slc25a25 Knock-out Mice—The initial induction of *Slc25a25* in skeletal muscle of cold-stressed mice, the slight reduction in lean mass under low fat chow diet, and the increased oxygen consumption per g of lean mass in *Slc25a25*$^{-/-}$ mice suggested that skeletal muscle function was perturbed. The impact of the deletion in *Slc25a25* on skeletal muscle function was determined by subjecting *Slc25a25*$^{-/-}$ mice to a forced treadmill exercise test. Mice lacking *Slc25a25* expression showed less than half the running capacity of WT mice and heterozygotes had an intermediate phenotype (Fig. 5*A*). Fiber-type analysis in soleus muscle, composed of oxidative fibers, collected from mice 1 week after the endurance test showed no difference in quantity of type 1 and

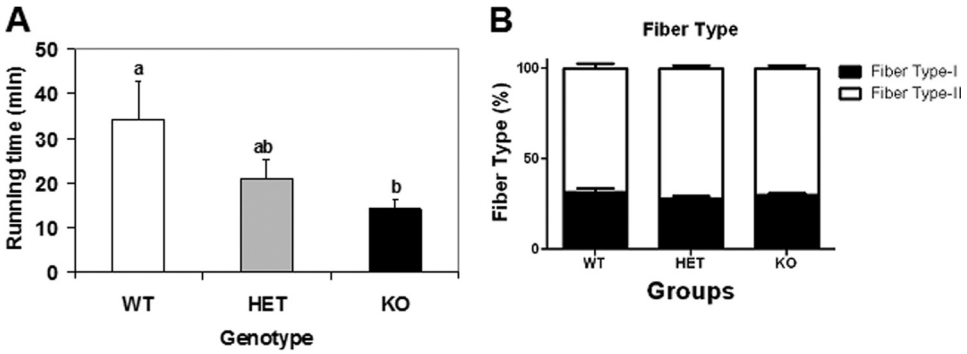

FIGURE 5. **Endurance phenotype and fiber-type distribution in *Slc25a25* wild-type and knock-out mice.** *A*, 12-week-old male *Slc25a25* wild-type ($n = 5$), heterozygous ($n = 5$), and knock-out ($n = 5$) mice were subjected to forced treadmill endurance test. *Slc25a25* knock-out mice have significantly reduced running time compared with wild-type mice. Data are mean ± S.E. *a* and *b,* statistically significant at $p < 0.05$. *B*, fiber type distribution in soleus muscle of *Slc25a25* wild-type ($n = 5$), heterozygous ($n = 5$), and knock-out ($n = 5$) mice. Samples were collected 1 week post-endurance test. No significant difference in distribution of type 1 and type 2 fibers was observed.

type 2 fibers (Fig. 5*B*) indicating that loss of SLC25A25 did not affect skeletal fiber type distribution. Mitochondrial content estimated by citrate synthase activity in mitochondrial preparations isolated from the gastronemius and quadriceps skeletal muscle was not different between the wild type and knock-out mice (data not shown). Immunoblot analysis of the composition of the respiratory complexes from mitochondria isolated from the quadriceps femoris with the MS604 antibody mixture from Mitosciences, Inc. (Eugene, OR) showed no differences in composition between wild type and mutant mice when fed a low fat chow diet or a high fat diet (data not shown). The hearts of SLC25A25-deficient mice have normal size (% of body weight: 0.65 ± 0.02 in WT *versus* 0.64 ± 0.03 in *Slc25a25*$^{-/-}$) and do not show evidence of hypertrophy. Thus disruption of *Slc25a25* function leads to a compromised muscle function under conditions of forced physical exertion. At present we do not know whether the difference in physical endurance is a consequence of skeletal or heart muscle function.

SLC25A25-deficient Mouse Embryonic Fibroblasts Show Reduced Ca^{2+} Flux and ATP Content—Based upon the fact that SLC25A25 has Ca^{2+}-binding EF-hand domains and its ATP-Mg^{2+}/P_i activity is regulated by Ca^{2+} (24), we next compared Ca^{2+} mobilization in MEF from WT and *Slc25a25*$^{-/-}$ mice. Cells were exposed to 300 nM bradykinin, an agonist of phospholipase C-coupled bradykinin receptor, to trigger Ca^{2+} release from the endoplasmic reticulum (ER). Bradykinin application induced a Ca^{2+} flux that was significantly less in mutant than WT MEF (area under the curve: 1,141,495 relative fluorescence units in WT *versus* 1,044,953 relative fluorescence units in *Slc25a25*$^{-/-}$, $p < 0.05$), indicating a difference in the filling state of the ER Ca^{2+} stores (Fig. 6*A*). Ca^{2+} flux in response to thapsigargin (Fig. 6*A*), a SERCA inhibitor, and ionomycin (Fig. 6*A*), an ionophore that induces pore formation in the endoplasmic reticulum membrane, did not show differences between WT and mutant *Slc25a25* MEF. Our study shows that the genetic manipulation of the transporter does not have any effect on calcium entry but does have an effect on ER calcium accumulation.

To identify bioenergetic defects incurred by inactivation of *Slc25a25*, we used an assay for mitochondrial function previously described (17, 18). MEF established from *Slc25a25* WT and knock-out mice were exposed to oligomycin (inhibitor of ATP synthase), FCCP (a protonophore and uncoupler of electron transport), antimycin A/rotenone (mitochondrial complex III/complex I inhibitor, respectively). The rate of basal respiration was 11% lower in *Slc25a25*$^{-/-}$ MEF compared with WT (Fig. 6*B*). SLC25A25-deficient MEF, in an effort to compensate for lower basal respiration, had a significantly higher rate of glycolysis as shown by extracellular acidification rate measurements (Fig. 6*B*). Similarly, the oligomycin-sensitive oxygen consumption rate, which corresponds to respiration linked to ATP synthesis was also 10% less in SLC25A25-deficient MEF (Fig. 6, *B* and *C*) compared with WT. Respiration associated with proton leak and FCCP-stimulated maximal respiratory rate was indistinguishable between WT and SLC25A25-deficient MEF; however, non-mitochondrial respiration was 19% lower in mutant MEF (Fig. 6, *B* and *C*) compared with WT. Measurement of cellular ATP levels showed that the basal ATP levels are 11% lower in mutant MEF (Fig. 6*D*). Inhibition of ATP synthesis by oligomycin treatment and glycolysis by 2-deoxyglucose treatment showed that ATP levels are significantly lower in Slc25a25-deficient MEF (Fig. 6*D*). Treatment of cells with inhibitors did not reduce cell viability and the activity of the mitochondrial marker, citrate synthase, was similar. These findings suggest that overall cellular respiration in mutant MEF is significantly reduced and that these cells are unable to compensate for sufficient ATP production by increasing glycolysis in the face of reduced mitochondrial respiration. Therefore, disruption of *Slc25a25* leads to altered cellular metabolism characterized by reduction in total mitochondrial and non-mitochondrial respiration, which leads to reduction in ATP levels. This may have significant implications in the ability of SLC25A25-deficient mice to produce sufficient ATP under conditions of increased energy demand such as skeletal muscle contraction and thus is consistent with the reduced endurance phenotype earlier described. ATP-Mg^{2+}/P_i carriers possess Ca^{2+}-binding motifs facing the extramitochondrial space, which allows regulation of the carrier transport activity by cytosolic Ca^{2+} without the requirement of Ca^{2+} entry in the organelle (25). In SLC25A25-deficient cells, the reduced Ca^{2+} flux paralleled the decrease in the capacity for ATP synthesis.

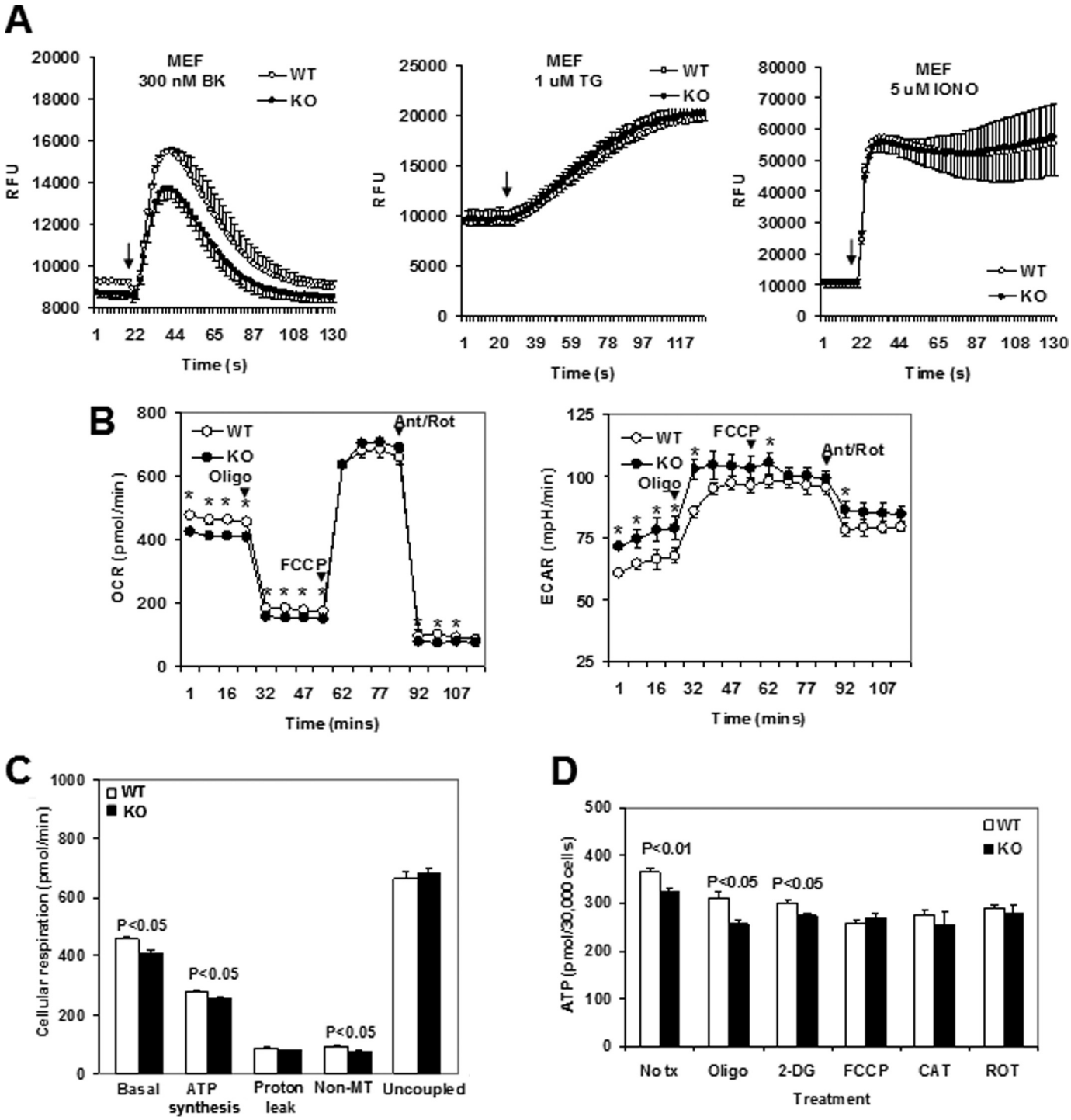

FIGURE 6. **Ca^{2+} flux and bioenergetic profile in MEF from *Slc25a25* wild-type and KO mice.** *A*, Ca^{2+} flux in WT and KO MEF exposed to 300 nM bradykinin, 1 μM thapsigargin, and 5 μM ionomycin. Data are from three independent experiments. Twenty replicates per genotype were used in each experiment. *B*, oxygen consumption rates (*OCR*) and extracellular acidification rates (*ECAR*) in WT and KO MEF. 5 μM oligomycin, 1 μM FCCP, and 1.5 μM antimycin A, 1 μM rotenone were injected at times indicated with measurements recorded after each injection. $p < 0.05$, *, WT *versus* KO. *C*, mitochondrial and non-mitochondrial respiration rates calculated from *B*. $p < 0.05$, Student's *t* test. *D*, cellular ATP levels in MEF at basal conditions and after a 1-min exposure to 5 μM oligomycin, 100 mM 2-deoxyglucose, 1 μM FCCP, 25 μM carboxyatractyloside, and 2 μM rotenone. All data presented are mean ± S.E.

Reduced Viability of $Slc25a25^{-/-}$·$Gdm^{-/-}$ Double Mutant Mice—Given the striking similarities in phenotypes of $Slc25a25^{-/-}$ and $Gdm^{-/-}$ mice, their Ca^{2+} binding domains and locations in the mitochondria, we used a number of different breeding strategies ($Slc25a25^{+/-}/Gdm^{+/-} \times Slc25a25^{+/-}/Gdm^{+/-}$, $Slc25a25^{+/-}/Gdm^{+/-} \times Slc25a25^{-/-}/Gdm^{+/-}$, $Slc25a25^{+/-}/Gdm^{-/-} \times Slc25a25^{+/-}/Gdm^{-/-}$ and $Slc25a25^{-/-}/Gdm^{+/-} \times Slc25a25^{-/-}/Gdm^{+/-}$) to generate $Slc25a25^{-/-}$·$Gdm1^{-/-}$ mice. Only 8 double mutants were obtained out of the expected 17 mice from a total of 159 offspring produced (χ square test, $p = 1.5 \times 10^{-8}$). Three of the 8 viable double mutants had observable abnormalities: 1 had a

unilateral cataract, another was runted, and 1 was found dead shortly after weaning. The reduction in viability of the *Slc25a25*$^{-/-}$·*Gdm1*$^{-/-}$ suggests that inactivation of both genes in a mouse disrupts mitochondrial function to a degree that survival is affected.

DISCUSSION

The phenotypes of *Slc25a25*$^{-/-}$ mice, resistance to diet-induced obesity and reduced physical endurance on a treadmill, are both consistent with reduced metabolic efficiency. The latter fits into a model in which an inability to maintain ATP levels impairs Ca^{2+} cycling in the ER and the subsequent efficiency of muscle contraction. A similar explanation can also apply to the resistance to diet-induced obesity, which manifests itself over a period of months rather than the minutes of a treadmill stress test, that is, muscular activity for normal daily functioning of *Slc25a25*$^{-/-}$ mice is less efficient and requires more caloric energy, which becomes evident over several months through reduced fat stores. Reduced ATP levels estimated from oxygen consumption rates and direct measurements in MEF, as well as attenuation of bradykinin-stimulated Ca^{2+} cycling in MEF, support the phenotypic data indicating that the capacity for ATP synthesis is compromised by inactivation of *Slc25a25*.

The ATP-Mg^{2+}/P$_i$ Carrier Function and the SLC25A25 Mitochondrial Carrier—In the 1980s an ATP-Mg^{2+}/P_i carrier function, located on the inner mitochondrial membrane, was proposed to be involved in uptake and accumulation of adenine nucleotides in newborn rat liver (26). This ATP-Mg^{2+}/P_i carrier catalyzes an electroneutral exchange of ATP-Mg^{2+} for P_i (27) and it is not inhibited by carboxyatractyloside and therefore not a ADP/ATP translocator. Importantly, the ATP transport activity can be activated by cytosolic Ca^{2+} (28, 29) and because variations in the concentration of adenine nucleotides were shown to affect state 3 respiration and ATP synthase-F_0F_1 activity (26), it is plausible that this carrier plays an important function in the regulation of ATP homeostasis during skeletal muscle contraction. Although, a structural analysis of the purified ATP-Mg^{2+}/P_i carrier from the mitochondrial membrane has not been achieved (30), structural and functional evidence suggested that SLC25A25 has properties consistent with that of the ATP-Mg^{2+}/P_i carrier (31, 32). SLC25A25 is a member of a family of inner membrane mitochondrial carriers (MC) that function to shuttle metabolites, nucleotides, and cofactors between the cytosol and mitochondria. SLC25A25 belongs to a subgroup of SCaMCs (short calcium-binding MC) having a bipartite structure; the C-terminal half is homologous with MC family members and the N-terminal extension harbors EF-hand motifs (corresponding to α-helices E and F of parvalbumin, the archetypical calcium-binding protein) (11). The extensions, which face the inter-membrane space, enable CaMCs to transduce Ca^{2+} signals without the need of Ca^{2+} uptake into the mitochondrial matrix. These structural properties, together with the fact that SLC25A25 is expressed at much higher levels in skeletal muscle than in liver or adipose tissue suggest an important function in controlling ATP and Ca^{2+} homeostasis in muscle.

Metabolic Inefficiency from Over- and Underexpression of Slc2a25—A challenge toward understanding the function of SLC25A25 in energy metabolism lies in explaining how both overexpression and underexpression of *Slc25a25* leads to reduced metabolic efficiency in mice fed an obesogenic diet. *Slc25a25* is overexpressed in mouse models of thermogenic deficiency when they are acutely exposed to an ambient temperature of 5 °C and cannot maintain normal body temperature (Fig. 1). We have reasoned that the maintenance of body temperature in the mouse is so critical to its survival that it was necessary to evolve a highly efficient system for the production, regulation, and distribution of heat, that is, brown adipose tissue. Therefore, if brown fat thermogenesis is inactivated by mutations to *Ucp1*, then alternative thermogenesis must be activated. As *Slc25a25*, which encodes a mitochondrial membrane protein associated with ATP regulation, was one of the major genes up-regulated in skeletal muscle in three models of cold-sensitive UCP1-deficient mice (Fig. 1), it became a candidate for alternative thermogenesis. To support this correlative data on induced overexpression implicating SLC25A25 in thermogenesis, we sought additional correlative data by producing mice with an inactivated *Slc25a25* gene. Similar to *Ucp1*$^{-/-}$ mice, *Slc25a25*$^{-/-}$ mice are resistant to diet-induced obesity, but unlike *Ucp1*$^{-/-}$ mice, resistance to diet-induced obesity is independent of the ambient temperature, that is, *Slc25a25*$^{-/-}$ mice are resistant to diet-induced obesity after the ambient temperature was increased to 28 °C (Fig. 3*B*). Therefore, *Slc25a25*$^{-/-}$ are metabolically inefficient (Table 2), but the source of inefficiency is not from a primary function in thermoregulation, because *Slc25a25*$^{-/-}$ mice maintain body temperature upon acute exposure to the cold (data not shown). Rather, the role of SLC25A25 in metabolic efficiency is most likely linked to the reduced efficiency of muscle function as evident from the physical endurance test of *Slc25a25*$^{-/-}$ mice on a treadmill. Accordingly, in the absence of SLC25A25 the efficiency of ATP production required for skeletal muscle function is diminished with secondary effects on adiposity.

The ultimate underlying cause for reduced muscle endurance lies in a reduced capacity for ATP synthesis (33). Indeed our studies on mitochondrial respiration in MEF from wild type and *Slc25a25*$^{-/-}$ mice show reduced basal and oligomycin-sensitive respiration in MEF from KO mice, as well as reduced ATP levels estimated by the luciferase/luciferin assay (Fig. 6). Consistent with this reduced ATP synthesis activity, Ca^{2+} cycling is attenuated in MEF of SLC25A25-deficient mice stimulated with bradykinin. During the muscle contraction process in *Slc25a25* mutants forced to exercise on a treadmill, it is possible that the reduced capacity for ATP synthesis cannot support activity of SERCA to maintain the sarcoplasmic reticulum Ca^{2+} pool. With time, insufficient Ca^{2+} will be released via the Ca^{2+} release channels impairing cross-bridge cycling causing diminished power output or muscle fatigue. In human patients with reduced Ca^{2+} sensitivity of force, a higher myoplasmic Ca^{2+} concentration is required to activate skeletal muscle fibers at the same level as controls through increased SERCA activity, thereby, diminishing the efficiency of muscle contraction (34).

Although the EF-hand structural domains of SLC25A25 suggest a function in Ca^{2+} metabolism, the reduced levels of ATP may affect muscle performance through reduced myosin activity. If reduced myosin activity occurs, the potential effects of reduced ATP production in SLC25A25-deficient mice may also extend to myosin-dependent skeletal muscle shivering. Shivering is thought to be the first line of defense to avoid a reduction in core temperature upon acute exposure to the cold, with induction of non-shivering thermogenesis subsequently being the main defense during chronic cold exposure (35). Several genetic models of mice with defective brown adipose tissue thermogenesis, *e.g.* UCP1 (21), acyl-CoA dehydrogenases (36), dopamine β-hydroxylase (37), or leptin (20), are cold intolerant during acute exposure to an ambient temperature of 4 °C, which suggests that shivering is incapable of maintaining body temperature in the acute phase. However, all of these mutants can tolerate the cold if gradually adapted by slowly lowering the ambient temperature (22, 23, 38). So what is the thermogenic mechanism in the brown adipose tissue-deficient cold adapted mice? The induction of *Slc25a25* in skeletal muscle of mice chronically exposed to the cold suggests it could contribute to adaptive thermogenesis in muscle. Given that its absence leads to accelerated muscle fatigue, it is worthwhile to consider whether SLC25A25 may be involved not only providing energy for muscle contraction associated with physical activity, but also with that associated with shivering and the possibility that there is an adaptive aspect to shivering associated with chronic exposure to cold.

Similarities between Gdm and Slc25a25—There is a remarkable similarity in the phenotypes of *Slc25a25*$^{-/-}$ and *Gdm*$^{-/-}$ mice that we and others have described (13, 39). Both mice have reduced lean mass, both maintain body temperature during an acute exposure to the cold at 4 °C, and both show the same adiposity profile during feeding of a high fat diet, first at 20 °C for 10 weeks and then at 28 °C for 10 weeks. Both mutant mice show increased oxygen consumption per g of lean mass when they are cold stressed. In addition, double mutant *Slc25a25*$^{-/-}$·*Gdm*$^{-/-}$ mice are obtained below the expected Mendelian ratios in appropriate crosses. One phenotypic difference is that *Gdm*$^{-/-}$ mice do not show reduced physical endurance.[5] There are also striking structural similarities, both proteins are located on the inner mitochondrial where they have EF-hand Ca^{2+}-binding domains facing the cytoplasmic space (11, 40). These enzymatic and transport activities and the molecular structures of SLC25A25 and GDM, together with the phenotypes of *Slc25a25*$^{-/-}$ mice, suggest a model in which both proteins are located in the inner mitochondrial membranes where their EF-hand Ca^{2+}-binding domains sense fluctuating Ca^{2+} and ATP concentrations associated with muscle contraction (Fig. 7).

In summary, the ability of UCP1-deficient mice to adapt to cold led us to search for an alternative thermogenic system. A microarray experiment of RNA from *Ucp1*$^{-/-}$ and wild type mice identified *Slc25a25* as a promising candidate. The phenotypes of *Slc25a25*$^{-/-}$ mice reveals that SLC25A25 is located in the inner mitochondria where its absence perturbs both mitochondrial respiration and Ca^{2+} cycling in the ER with effects on skeletal muscle function. Furthermore, the loss of SLC25A25 activity has effects on systemic energy balance as indicated by the resistance of *Slc25a25*$^{-/-}$ mice to diet-induced obesity. These studies on a role for mitochondrial Ca^{2+} proteins in muscle dovetail with a recently described role for an ATP-sensitive K^+ channel protein (Kir6.2) in energy homeostasis as evidence by a resistance to obesity and reduced muscle endurance in the Kir6.2-deficient mice (41, 42). These phenotypes of *Slc25a25*$^{-/-}$ and *Kir6.2*$^{-/-}$ mice point to a pivotal role for these proteins in systemic energy balance as well as muscle function.

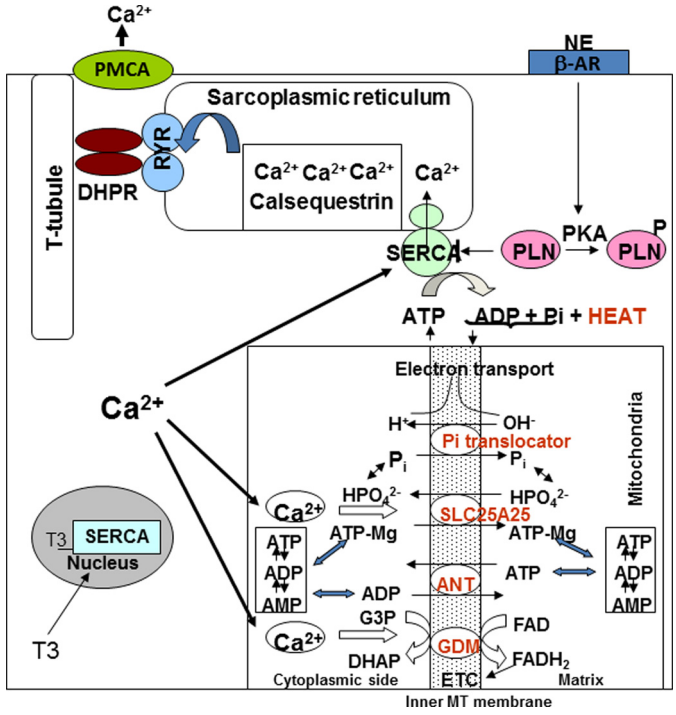

FIGURE 7. **Model of *Slc25a25* and *Gdm*-mediated regulation of energy metabolism.** SLC25A25 and Gdm are located in the inner mitochondrial membrane where they function through their Ca^{2+}-binding domains to coordinate requirements for ATP production to support Ca^{2+} pumping by SERCA from the cytoplasm to the sarcoplasmic reticulum. Inactivation of one or both of these genes is proposed to effect ATP production with downstream effects on metabolic efficiency as evident from physical activity monitored on a treadmill and regulation of energy balance under cold stress. Modified from models published by Block (43) and Aprille (44).

Acknowledgements—We thank Tamra Mendoza and Cody Giardina for excellent technical assistance. This work used the Genomics and Cell Biology an Bioimaging core facilities supported in part by the Nutrition Obesity Research Center Grant 1P30 DK07246 and COBRE (National Institutes of Health Grant P20-TT021925).

REFERENCES

1. Morton, G. J., Cummings, D. E., Baskin, D. G., Barsh, G. S., and Schwartz, M. W. (2006) *Nature* **443,** 289–295
2. Hawley, J. A., and Holloszy, J. O. (2009) *Nutr. Rev.* **67,** 172–178
3. Kozak, L. P. (2010) *Cell Metab.* **11,** 263–267
4. Zurlo, F., Lillioja, S., Esposito-Del Puente, A., Nyomba, B. L., Raz, I., Saad, M. F., Swinburn, B. A., Knowler, W. C., Bogardus, C., and Ravussin, E. (1990) *Am. J. Physiol. Endocrinol. Metab.* **259,** E650-E657
5. Lowell, B. B., and Shulman, G. I. (2005) *Science* **307,** 384–387
6. Kranias, E. G., and Bers, D. M. (2007) *Subcell. Biochem.* **45,** 523–537
7. MacLennan, D. H. (2000) *Eur. J. Biochem.* **267,** 5291–5297
8. Periasamy, M., Reed, T. D., Liu, L. H., Ji, Y., Loukianov, E., Paul, R. J.,

Nieman, M. L., Riddle, T., Duffy, J. J., Doetschman, T., Lorenz, J. N., and Shull, G. E. (1999) *J. Biol. Chem.* **274,** 2556–2562
9. Handschin, C., Choi, C. S., Chin, S., Kim, S., Kawamori, D., Kurpad, A. J., Neubauer, N., Hu, J., Mootha, V. K., Kim, Y. B., Kulkarni, R. N., Shulman, G. I., and Spiegelman, B. M. (2007) *J. Clin. Invest.* **117,** 3463–3474
10. Liu, X., Rossmeisl, M., McClaine, J., Riachi, M., Harper, M. E., and Kozak, L. P. (2003) *J. Clin. Invest.* **111,** 399–407
11. Satrústegui, J., Pardo, B., and Del Arco, A. (2007) *Physiol. Rev.* **87,** 29–67
12. Lakso, M., Pichel, J. G., Gorman, J. R., Sauer, B., Okamoto, Y., Lee, E., Alt, F. W., and Westphal, H. (1996) *Proc. Natl. Acad. Sci. U.S.A.* **93,** 5860–5865
13. Anunciado-Koza, R., Ukropec, J., Koza, R. A., and Kozak, L. P. (2008) *J. Biol. Chem.* **283,** 27688–27697
14. Koza, R. A., Nikonova, L., Hogan, J., Rim, J. S., Mendoza, T., Faulk, C., Skaf, J., and Kozak, L. P. (2006) *PLoS Genet.* **2,** e81
15. Koza, R. A., Hohmann, S. M., Guerra, C., Rossmeisl, M., and Kozak, L. P. (2000) *J. Biol. Chem.* **275,** 34486–34492
16. Wu, M., Neilson, A., Swift, A. L., Moran, R., Tamagnine, J., Parslow, D., Armistead, S., Lemire, K., Orrell, J., Teich, J., Chomicz, S., and Ferrick, D. A. (2007) *Am. J. Physiol. Cell Physiol.* **292,** C125–136
17. Amo, T., Yadava, N., Oh, R., Nicholls, D. G., and Brand, M. D. (2008) *Gene* **411,** 69–76
18. Hill, B. G., Dranka, B. P., Zou, L., Chatham, J. C., and Darley-Usmar, V. M. (2009) *Biochem. J.* **424,** 99–107
19. Bajpeyi, S., Tanner, C. J., Slentz, C. A., Duscha, B. D., McCartney, J. S., Hickner, R. C., Kraus, W. E., and Houmard, J. A. (2009) *J. Appl. Physiol.* **106,** 1079–1085
20. Trayhurn, P., and James, W. P. (1978) *Pflugers Arch.* **373,** 189–193
21. Enerbäck, S., Jacobsson, A., Simpson, E. M., Guerra, C., Yamashita, H., Harper, M. E., and Kozak, L. P. (1997) *Nature* **387,** 90–94
22. Ukropec, J., Anunciado, R. V., Ravussin, Y., and Kozak, L. P. (2006) *Endocrinology* **147,** 2468–2480
23. Ukropec, J., Anunciado, R. P., Ravussin, Y., Hulver, M. W., and Kozak, L. P. (2006) *J. Biol. Chem.* **281,** 31894–31908
24. Del Arco, A. (2005) *Biochem. J.* **389,** 647–655
25. Cavero, S., Traba, J., Del Arco, A., and Satrustegui, J. (2005) *Biochem. J.* **392,** 537–544
26. Aprille, J. R. (1988) *FASEB J.* **2,** 2547–2556
27. Joyal, J. L., and Aprille, J. R. (1992) *J. Biol. Chem.* **267,** 19198–19203
28. Haynes, R. C., Jr., Picking, R. A., and Zaks, W. J. (1986) *J. Biol. Chem.* **261,** 16121–16125
29. Nosek, M. T., Dransfield, D. T., and Aprille, J. R. (1990) *J. Biol. Chem.* **265,** 8444–8450
30. Pollak, J. K., and Sutton, R. (1980) *Biochem. J.* **192,** 75–83
31. Kunji, E. R. (2004) *FEBS Lett.* **564,** 239–244
32. Palmieri, F. (2004) *Pflugers Arch.* **447,** 689–709
33. Holloszy, J. O., and Booth, F. W. (1976) *Annu. Rev. Physiol.* **38,** 273–291
34. Ochala, J., Carpén, O., and Larsson, L. (2009) *Ups. J. Med. Sci.* **114,** 235–241
35. Hemingway, A. (1963) *Physiol. Rev.* **43,** 397–422
36. Guerra, C., Koza, R. A., Walsh, K., Kurtz, D. M., Wood, P. A., and Kozak, L. P. (1998) *J. Clin. Invest.* **102,** 1724–1731
37. Thomas, S. A., and Palmiter, R. D. (1997) *Nature* **387,** 94–97
38. Golozoubova, V., Hohtola, E., Matthias, A., Jacobsson, A., Cannon, B., and Nedergaard, J. (2001) *FASEB J.* **15,** 2048–2050
39. Brown, L. J., Koza, R. A., Everett, C., Reitman, M. L., Marshall, L., Fahien, L. A., Kozak, L. P., and MacDonald, M. J. (2002) *J. Biol. Chem.* **277,** 32892–32898
40. Brown, L. J., MacDonald, M. J., Lehn, D. A., and Moran, S. M. (1994) *J. Biol. Chem.* **269,** 14363–14366
41. Alekseev, A. E., Reyes, S., Yamada, S., Hodgson-Zingman, D. M., Sattiraju, S., Zhu, Z., Sierra, A., Gerbin, M., Coetzee, W. A., Goldhamer, D. J., Terzic, A., and Zingman, L. V. (2010) *Cell Metab.* **11,** 58–69
42. Costanzo-Garvey, D. L., Pfluger, P. T., Dougherty, M. K., Stock, J. L., Boehm, M., Chaika, O., Fernandez, M. R., Fisher, K., Kortum, R. L., Hong, E. G., Jun, J. Y., Ko, H. J., Schreiner, A., Volle, D. J., Treece, T., Swift, A. L., Winer, M., Chen, D., Wu, M., Leon, L. R., Shaw, A. S., McNeish, J., Kim, J. K., Morrison, D. K., Tschöp, M. H., and Lewis, R. E. (2009) *Cell Metab.* **10,** 366–378
43. Block, B. A. (1994) *Annu. Rev. Physiol.* **56,** 535–577
44. Aprille, J. R. (1993) *J. Bioenerg. Biomembr.* **25,** 473–481